BIOCHEMISTRY
including biophysical chemistry & molecular biology
Article

Biochemistry **2010,** *49,* 6519–6530 6519
DOI: 10.1021/bi100578x

Factors Defining Effects of Macromolecular Crowding on Protein Stability: An in Vitro/in Silico Case Study Using Cytochrome *c*†

Alexander Christiansen,‡ Qian Wang,§ Antonios Samiotakis,§ Margaret S. Cheung,§ and Pernilla Wittung-Stafshede*,‡

‡*Department of Chemistry, Chemical Biological Center, Umea University, 901 87 Umea, Sweden, and* §*Department of Physics, University of Houston, Houston, Texas 77204*

Received April 15, 2010; Revised Manuscript Received June 24, 2010

ABSTRACT: Previous experiments with two single-domain proteins showed that macromolecular crowding can stabilize dramatically toward heat perturbation and modulate native-state structure and shape. To assess the generality of this, we here tested the effects of the synthetic crowding agents on cytochrome *c*, a small single-domain protein. Using far-UV circular dichroism (CD), we discovered that there is no effect on cytochrome *c*'s secondary structure upon addition of Ficoll or dextran (0−400 mg/mL, pH 7). Thermal experiments revealed stabilizing effects (5−10 °C) of Ficoll 70 and dextran 70; this effect was enhanced by the presence of low levels of guanidine hydrochloride (GuHCl) that destabilize the protein. When using a smaller dextran, dextran 40, the thermal effects were larger (10−20 °C). In silico analysis, using structure-based (Go-like) interactions for cytochrome *c*, is in excellent agreement with the in vitro thermodynamic data and also agrees with scaled particle theory. Simulations of a range of crowder size and shape demonstrated that the smaller the crowder the larger the favorable effect on cytochrome *c*'s folded-state stability. Together with previous data, we conclude that protein size, stability, conformational malleability, and folding routes, as well as crowder size and shape, are key factors that modulate the net effect of macromolecular crowding on proteins.

It is most often assumed that protein biophysical and structural properties observed in dilute buffer solutions in vitro also represent the in vivo scenario. However, the intracellular environment is highly crowded because of the presence of large amounts of soluble and insoluble biomolecules, including proteins, nucleic acids, ribosomes, and carbohydrates. This means that a significant fraction of the intracellular space is not available to other macromolecular species. It has been estimated that the concentration of macromolecules in the cytoplasm ranges from 80 to 400 mg/mL (*1*). All macromolecules in physiological fluids collectively occupy between 10 and 40% of the total aqua-based volume (*2*). The term "macromolecular crowding", coined by Minton (*3*), implies the nonspecific influence of steric repulsions on specific reactions that occur in highly volume-occupied media. Because of excluded volume effects (*4*), any reaction that amplifies the available volume will be stimulated by macromolecular crowding (*5*). It is proposed that crowding provides a stabilizing effect to the folded state of proteins indirectly due to compaction of the more extended and malleable denatured states (*6*, *7*).

Macromolecular crowding effects have also been extended to structural compression in nucleic acids (*8*), and comparisons between crowding and confinement effects were conducted with sol−gel experiments nearly a decade ago (*9*). As a result of recent advances in computational methods and resources, investigations of confinement and macromolecular crowding effects on protein conformational changes (*10*, *11*), folding (*12*, *13*), thermodynamics and kinetics of protein folding under confinement (*14*), association (*15*, *16*), and dynamics (*17*) have improved our understanding of biopolymer dynamics under cell-like conditions.

Macromolecular crowding in solution can be mimicked experimentally via addition of high concentrations of inert synthetic or natural macromolecules, termed crowding agents, to the systems in vitro. Experimental and theoretical work has demonstrated large effects of macromolecular crowding on many biological processes in solution (*7*). Whereas theoretical simulations have focused on small proteins or peptides (*7*), experimental crowding studies in solution have mostly involved large, complex proteins (i.e., multidomain and/or disulfide-containing) and often extreme solvent conditions (such as acidic pH). A few studies have also focused on the ability of crowding agents to induce conformational changes in unfolded states of proteins (*18*, *19*). We recently combined in vitro spectroscopic experiments and computer simulations to reveal effects of macromolecular crowding on α/β *Desulfovibrio desulfuricans* apoflavodoxin (148 residues) and α-helical VlsE (327 residues) at neutral pH. Surprisingly, both proteins become more structured in their folded states because of crowding: VlsE, being aspherical, underwent a change in folded-state shape under crowded conditions (*20*−*22*). In agreement with predictions based on the excluded volume interactions exerted by crowders, both proteins were thermally stabilized by the presence of crowding agents; in the case of apoflavodoxin, the effects were rather dramatic (up to 20 °C).

To test the generality of our previous results and to increase the size of the database of proteins tested experimentally for crowding effects, we here studied in vitro and in silico the effects of macromolecular crowding on the structure and stability of the

†P.W.-S. acknowledges funds from the Kempe and Wallenberg foundations and the Swedish Research Council. M.S.C. is supported by the National Science Foundation (MCB 0919974) and the University of Houston.

*To whom correspondence should be addressed: Department of Chemistry, Chemical Biological Center, Umea University, 901 87 Umea, Sweden. Phone: +46-90-7865347. Fax: +46-90-7867655. E-mail: pernilla.wittung@chem.umu.se.

Published on Web 07/01/2010

single-domain protein horse heart cytochrome *c* (helical structure, 104 residues) that folds with an apparent two-state equilibrium mechanism in dilute solutions (like flavodoxin and VlsE). Nonetheless, cytochrome *c* is smaller in size and more stable in vitro than the previously studied proteins. We discovered both in vitro and in silico that (in contrast to flavodoxin and VlsE) there is no change in the folded-state structure induced by either Ficoll or dextran, although cytochrome *c* is thermally stabilized by the crowding agents. Modulating cytochrome *c*'s stability with GuHCl[1] revealed that crowding effects on thermal stability are enhanced when the protein is destabilized. In addition, systematic simulations showed that the smaller the crowder, the larger the effect on cytochrome *c*'s stability. Taken together, we propose that protein size and stability, as well as the size and shape of the crowding agents, are key factors that will dictate the absolute effects of macromolecular crowding on protein stability in vivo.

MATERIALS AND METHODS

Experimental Procedures. Lyophilized horse heart cytochrome *c* (Sigma) was dissolved in 20 mM phosphate (pH 7.0) without further purification. The protein concentration was determined using heme absorption at 409 nm (ε_{409} = 106000 mol^{-1} cm^{-1}). Ficoll 70, dextran 70, and dextran 40 (all from Sigma, highest grade) were dissolved in 20 mM phosphate buffer (pH 7.0). GuHCl (Sigma) solutions were prepared in 20 mM phosphate buffer (that was brought to pH 7.0); the concentration was determined with a Zeiss refractometer. To check for the presence of contaminating reduced sugars (e.g., glucose) in the Ficoll and dextran solutions, an assay using 3,5-dinitrosalycilic (Sigma) described by Miller (*23*) was used with some modifications. In none of the macromolecular crowding agent solutions was the content of reducing sugar molecules greater than 0.1%.

Samples of 10 μM cytochrome *c* [in 20 mM phosphate buffer (pH 7)] at different concentrations (0−400 mg/mL) of Ficoll 70, dextran 40, or dextran 70 were prepared and equilibrated for 1 h at 20 °C. Far-UV circular dichroism (CD) spectra (210−260 nm) and near-UV−visible CD spectra (280−600 nm) of the protein samples were collected on a Chirascan (Applied Photophysics) CD spectropolarimeter with a 1 nm data interval at 20 °C in a 1 mm cell. All reported spectra are averages of three spectra after subtraction of the buffer signal and baseline correction. Thermally induced unfolding of cytochrome *c* (pH 7.0) in the presence and absence of macromolecular crowding agents or sucrose (in the presence of various concentrations of GuHCl) was monitored via CD at 220 nm from 20 to 90 °C with a scan rate of 1 °C/min. Far-UV CD spectra of unfolded cytochrome *c* were recorded at the highest temperature using the same parameters given above for the folded protein.

The reversibility of the thermal transitions was checked by first performing the thermal unfolding to the point where the post-transition baseline starts. The sample was then allowed to cool to the starting temperature (20 °C), after which a far-UV CD spectrum was recorded. The intensity and shape of the spectra before and after heating were then compared. In all cases, the reversibility of the thermal transitions was greater than 80%. The thermal unfolding curves were fitted to a modified form of the van't Hoff equation, which simultaneously fits the folded and unfolded baselines and the transition region to produce the thermal midpoint (T_m) and enthalpy of unfolding [$\Delta H(T_m)$] values for unfolding under each solvent condition (*24*, *25*) (examples of raw data overlaid with fits are shown in Figure S1 of the Supporting Information):

$$y = y_f + m_f T + (y_u + m_u T)[K_U/(1 + K_U)]$$

where

$$K_U = \exp[-\Delta H(1 - T/T_m)/(RT)]$$

where y is the spectroscopic signal, m_f and m_u are the slopes and y_f and y_u the intercepts of the folded- and unfolded-state baselines, respectively, T is the temperature, and K_U is the unfolded−folded equilibrium constant. Data were fitted using Origin version 6. T_m and $\Delta H(T_m)$ values are listed in Table 1 for ΔH and Table S1 of the Supporting Information for T_m; errors given are standard errors from the fits. For several conditions, more than one measurement was taken and statistical error analysis of ΔH values from these data sets is given in Table S3 of the Supporting Information. Fluorescence measurements were performed on a Cary Eclipse spectrofluorimeter. Emission at 20 °C (excitation at 285 nm) was recorded from 310 to 460 nm with a 1 nm data interval (1 cm cell). Thermal unfolding of cytochrome *c* in different crowding agents was measured by fluorescence at 350 nm (excitation at 285 nm) while the sample was heated (1 °C/min).

Chemical denaturation of cytochrome *c* (without or with 300 mg/mL Ficoll 70) was performed at 20 °C (pH 7.0) using GuHCl

Table 1: $\Delta H(T_m)$ Values in Kilojoules per Mole for Cytochrome *c* (pH 7) in the Presence of Various Levels of Ficoll 70, Dextran 40, and Dextran 70, Obtained upon Two-State Analysis of Thermal Transitions[a]

[GuHCl] (M)	buffer	200 mg/mL	300 mg/mL	400 mg/mL
		Ficoll 70		
0.50	340 ± 16	365 ± 7	327 ± 9	425 ± 7
0.75	318 ± 10	319 ± 7	307 ± 6	311 ± 8
1.00	320 ± 7	289 ± 5	287 ± 4	336 ± 5
1.25	266 ± 7	276 ± 6	241 ± 6	291 ± 8
1.50	257 ± 7	258 ± 5	262 ± 6	260 ± 6
1.60	242 ± 7	−	226 ± 7	216 ± 6
1.75	205 ± 5	234 ± 4	240 ± 5	256 ± 4
		Dextran 70		
0.50	344 ± 14	370 ± 21	273 ± 25	348 ± 33
0.75	321 ± 10	294 ± 15	291 ± 18	313 ± 21
1.00	318 ± 10	283 ± 11	296 ± 15	321 ± 17
1.25	265 ± 9	290 ± 12	276 ± 14	291 ± 11
1.50	254 ± 8	194 ± 11	251 ± 19	253 ± 9
1.60	225 ± 8	248 ± 10	240 ± 13	222 ± 17
1.75	204 ± 3	234 ± 9	201 ± 6	−
		Dextran 40		
0.50	344 ± 14	301 ± 16	289 ± 22	299 ± 22
0.75	321 ± 10	328 ± 15	369 ± 25	225 ± 18
1.00	318 ± 10	270 ± 10	276 ± 10	260 ± 20
1.25	265 ± 9	269 ± 10	257 ± 10	200 ± 15
1.50	254 ± 8	255 ± 8	233 ± 10	199 ± 10
1.60	225 ± 8	243 ± 8	243 ± 10	230 ± 8
1.75	204 ± 3	219 ± 7	243 ± 10	227 ± 7

[a]Examples of transitions shown in Figure 1A; midpoint T_m values plotted in Figure 1B−D and listed in Table S1 of the Supporting Information. The GuHCl concentrations are uncorrected (see Table S2 of the Supporting Information for corrected GuHCl values at each crowding agent concentration). Standard errors in $\Delta H(T_m)$ are taken from the fits (see also Table S3 of the Supporting Information for further statistical analysis).

[1]Abbreviations: CD, circular dichroism; T_m, thermal midpoint; SPT, scaled particle theory; GuHCl, guanidine hydrochloride; PDB, Protein Data Bank.

(in 0.5 M increments) as the denaturant. Samples were incubated for 1 h before measurements. Unfolding was followed by far-UV CD and fluorescence detection using the same parameters used for for the spectra described above. The signals at 220 nm (CD) or 350 nm (fluorescence) were fitted to a two-state model to obtain the midpoint of unfolding (*26*) (Figure S2 of the Supporting Information). The two isothermal unfolding curves were used to determine what GuHCl concentrations to utilize in the thermal experiments (i.e., GuHCl levels that destabilize the folded protein but do not cause any changes in the protein secondary structure at 20 °C.)

GuHCl Concentration Corrections Due to Solvent-Excluded Volume. An inert crowding agent increases the concentration of any small solute by decreasing its available volume through steric repulsion (assuming no interactions between the crowding agent and the solute) (*27*−*29*). The GuHCl concentrations in the cytochrome *c* samples were therefore corrected ($[GuHCl]_{corr}$) to account for the solvent-excluded volume due to the presence of Ficoll or dextran. For this, we determined the value of Ficoll 70's partial specific volume to be 0.65 ± 0.02 mL/g. This value was found to be same for the two dextrans and did not depend on the amount of crowding agent dissolved (200−400 mg/mL). Moreover, the crowding agent's partial specific volume value was the same in buffer, in 0.5−6 M GuHCl, and in 8 M urea, indicating that there are no specific interactions between GuHCl or urea and Ficoll or dextran. For corrections, we used $[GuHCl]_{corr} = (1/f_{av})[GuHCl]$, where f_{av} is the volume fraction available to the solvent (*27*). For example, for 300 mg/mL Ficoll 70 solutions, $f_{av} \sim 0.8$ (i.e., 1 − 0.65 mL/g × 0.3 g/mL). All GuHCl concentrations used in thermal experiments and in the chemical denaturant experiment with 300 mg/mL Ficoll 70 were corrected in this way on the basis of the amount of crowding agent present. In Table S2 of the Supporting Information, corrected GuHCl concentrations are given for various starting GuHCl concentrations as a function of increasing levels of crowding agent.

Coarse-Grained Modeling of Cytochrome c and Heme. A side chain C_α model (SCM) that includes two beads per amino acid (except glycine) was used to represent the protein structure of cytochrome *c*, and a description of the structural Hamiltonian in this model was presented in ref *30*. A structure-based (i.e., Go-type) energy function was implemented for the nonbonded interactions on cytochrome *c* in which only the contact formations in the crystal structure (PDB entry 1HRC) determined by X-ray diffraction were attractive, and its description appears in ref *30* .

The model of cytochrome *c*'s heme that we used was modified from the coarse-grained heme model used in the computational study by Wolynes' group (*31*), in which a square planar placement of four beads is used to represent the heme. We took the positions of the four nitrogen atoms (labeled NA, NB, NC, and ND) from the crystal structure of cytochrome *c* (PDB entry 1HRC). These were used to create our heme model with four pseudobeads (named H_m, where $m = 1, 2, 3,$ or 4) with the radius of 5 Å that minimized steric clashes. The four H_m pseudobeads are interconnected with harmonic interactions (eq 1), a total of six bonds, to maintain a planar geometry. In addition, each H_m bead is connected to the side chain bead of His17 through a harmonic interaction by the following formula:

$$E^{ij}_{\text{bond}} = k_b(r^{ij} - r^{ij}_0)^2 \quad (1)$$

where i and $j \in H_m$ or $i \in H_m$ and j is the side chain bead of His17. $k_b = 100\varepsilon$, and $\varepsilon = 0.6$ kcal/mol. r^{ij}_0 was calculated from the crystal structure of the heme of cytochrome *c*.

Each bond angle energy term for three adjacent beads across heme and His17 and heme i, j, and k in which i is the C_α bead of His17, j is the C_β bead of His17, and $k \in H_m$ is in the following form:

$$E^{ijk}_{\text{angle}} = k_\theta(\theta^{ijk} - \theta^{ijk}_0)^2 \quad (2)$$

where $k_\theta = 20\varepsilon$ and θ^{ijk}_0 values were calculated from the crystal structure of cytochrome *c*.

Each dihedral energy term for four consecutive beads across His17 and heme i, j, k, and l is defined in eq 3. i is the C_α bead of His17. j is the C_β bead of His17. k and l are heme beads, and both take the following values: $k = H_1$, $l = H_2$; $k = H_2$, $l = H_3$; $k = H_3$, $l = H_4$; $k = H_4$, $l = H_1$.

$$E^{ijkl}_{\text{dihedral}} = k_\phi[1 - \cos(\phi^{ijkl} - \phi^{ijkl}_0)] \quad (3)$$

where $k_\varphi = \varepsilon$ and ϕ^{ijkl}_0 values were calculated from the crystal structure of cytochrome *c*.

The nonbonded interactions between the coarse-grained protein and heme, E_{ph}, follow a Go-like (structure-based) potential in which only the ones found in the crystal structure are attractive. These contacts were defined by the program of Ligand-Protein Contacts (LPC software) (*32*). The behavior of these selected contacts follows a Lennard-Jones interaction in eq 4. i is a side chain bead, and $j \in H_m$

$$E^{ij}_{\text{ph}} = \varepsilon\left[\left(\frac{\sigma_{ij}}{r_{ij}}\right)^{12} - 2\left(\frac{\sigma_{ij}}{r_{ij}}\right)^{6}\right] \quad (4)$$

where $\varepsilon = 0.6$ kcal/mol and $\sigma_{ij} = f(\sigma_i + \sigma_j)$; σ_i and σ_j are the van der Waals radii of the interacting beads. $|i - j| > 1$. $f = 0.9$ is a scaling factor to prevent clashes between interacting beads. Nonnative interactions are strictly repulsive following

$$E^{ij}_{\text{non-native}} = \varepsilon\left(\frac{\sigma_{ij}}{r_{ij}}\right)^{12} \quad (5)$$

Coarse-Grained Modeling of Crowding Agents. Several types of crowders were used in computer simulations to address the effects of crowder size and shape variations on the folding energy landscapes (*7*, *21*, *33*). Four spherical crowding agents were used in the simulation: (a) Ficoll 70, a hard sphere with an R_g of 55 Å and a mass of 70 kDa; (b) CR-40, a hard sphere with an R_g of 45.5 Å and a 40 kDa mass equivalent to that of fictitious "Ficoll 40"; (c) CR-10, a hard sphere with an R_g of 28.5 Å and a 10 kDa mass called CR-10 equivalent to fictitious "Ficoll 10"; and (d) CR-cyt, a hard sphere with the size of folded cytochrome *c*, with an R^N_g of 13.1 Å. CR-cyt is the smallest crowder in the simulation (that is still not smaller than the size of a native protein). In addition, two dumbbell-shaped crowding agents were modeled: (e) Dumbbell 70, a dumbbell-shaped crowder created by using two hard-core Ficoll 70 spheres and linked by a harmonic bond whose equilibration length is 106.4 Å; and (f) SD-70, created by using two equally sized hard-core spheres whose total volume equals one Ficoll 70 linked by a harmonic bond whose equilibration length is 83.6 Å. We used volume fractions of crowders (φ_c) of 0% (bulk), 25%, and 40% for each type of crowder described above in the computer simulations.

Simulation Techniques. To study the thermodynamic properties of cytochrome *c* in silico, we used molecular simulations using Langevin equations of motion. An in-house developed

version of AMBER6 (*34*) in which the Langevin equations of motion were integrated in low-friction limit was used (*35*). The Replica Exchange Method (REM) (*36*) was implemented to enhance the sampling efficiency of the simulations on cytochrome *c*. The REM is a computational method that executes several copies of standard molecular simulations at different temperatures in a range from $0.97k_BT/\varepsilon$ to $1.50k_BT/\varepsilon$ simultaneously, and each copy attempts to communicate with another copy every certain time step through a rule based on the Metropolis criterion (*37*): the acceptance probability (P_{acc}) for the exchange of two neighboring replica copies, *i* and *j*, equals $\min(1,\exp\{(\beta_i - \beta_j)[U(r_i)-U(r_j)]\})$, where $\beta = 1/k_BT$ and $U(r)$ represented the configurational energy of the system. The acceptance ratio remained between 20% and 30% among the distribution of replicas at different temperatures. The integration time step is $10^{-4}\tau_L$, where $\tau_L = (m\sigma^2/\varepsilon)^{0.5}$. Each exchange was attempted at every $400\tau_L$. For our computations of thermodynamic values, a total of at least 40000 statistically significant conformations were collected from each replica copy, where the time separation of sampling is greater than one correlation time. Thermodynamic properties and errors were calculated using the weighted histogram analysis method (*38*).

Shape Analysis. The shape of configurations can be characterized by two rotationally invariant quantities, the asphericity (Δ) and the shape parameter (S) (*39*). S and Δ are determined from the inertia tensor, $\mathbf{T}_{\alpha\beta}$, in eqs 6−8:

$$\mathbf{T}_{\alpha\beta} = \frac{1}{2N^2}\sum_{i,j=1}^{N}(r_{i\alpha} - r_{j\alpha})(r_{i\beta} - r_{j\beta}) \quad (6)$$

where N is the total number of atoms and α and β represent the X, Y, and Z components. The eigenvalues of $\mathbf{T}$ are denoted by $\lambda_i (i = 1, 2, 3)$. $\bar{\lambda}$ is the average of λ_i values.

$$\Delta = \frac{3}{2}\frac{\sum_{i=1}^{3}(\lambda_i - \bar{\lambda})^2}{(trT)^2} \quad (7)$$

$$S = 27\frac{\prod_{i=1}^{3}(\lambda_i - \bar{\lambda})}{(trT)^3} \quad (8)$$

Asphericity (Δ) ranges from 0 to 1, and a Δ of 0 corresponds to a sphere. Deviation of Δ from 0 indicates the extent of anisotropy. The shape parameter (S) ranges from −0.25 to 2; a negative S corresponds to an oblate ellipsoid and a positive S to a prolate ellipsoid, whereas $S = 0$ is a sphere.

RESULTS

Choice of Protein and Crowding Agents. Cytochrome *c* was selected as target protein in this study because (a) it has been extensively characterized in dilute buffers (*40*−*45*), (b) it is a small single-domain protein that unfolds reversibly in vitro, and (c) the equilibrium unfolding mechanism in buffer appears to be a two-state mechanism. The crowding agents selected for this study are the sugar-based polymer Ficoll 70 (70 kDa; no other size is available) and dextrans 40 and 70 (40 and 70 kDa, respectively) because (a) they are believed to affect proteins via excluded volume effects, (b) they have low absorption above 200 nm, (c) they do not interact with proteins, (d) they are inert and do not have phase transitions in the temperature regions to be studied, and (e) Ficoll adopts a semirigid sphere shape (*46*−*49*) and can therefore easily be modeled in computations as hard spheres, whereas dextran can be modeled as a random array of rods in solution (*19*, *50*), approximated by short dumbbell models in our computer simulations.

Modulation of Thermal Stability by Crowding Agents. The thermal midpoint (T_m) for cytochrome *c* at physiological pH is ∼82 °C (*51*, *52*), and this reaction is not reversible in vitro. However, introduction of low levels of the chemical denaturant GuHCl results in cytochrome *c* destabilization (lowering the T_m), and the thermal process becomes reversible. All GuHCl concentrations in the presence of Ficoll or dextran were corrected as described in Materials and Methods for solvent-excluded volume due to the presence of the crowding agents (see Table S1 of the Supporting Information for a list of corrected GuHCl values). Thermal experiments probed by far-UV CD of cytochrome *c* in the presence of increasing GuHCl concentrations were performed in the presence and absence of 200, 300, and 400 mg/mL Ficoll 70 (∼70 kDa). All these reactions were more than 80% reversible. Addition of up to 2 M GuHCl in the absence of crowding agent does not cause any protein unfolding at 20 °C as concluded from the lack of changes in far-UV CD (secondary structure; see Figure S2 of the Supporting Information), Trp emission (Trp environment; Figure S3A of the Supporting Information), and visible CD (heme environment; see Figure S3B of the Supporting Information). However, GuHCl additions in this range destabilize cytochrome *c* such that the T_m is lowered. Chemical GuHCl-induced unfolding curves in buffer and in 300 mg/mL Ficoll 70 at 20 °C are shown in Figure S2 of the Supporting Information. The data demonstrate, in accord with the thermal data presented below, that there is a shift in cytochrome *c*'s unfolding midpoint toward higher GuHCl concentrations in the presence of Ficoll 70, but that the reaction remains two-state-like. This trend was shown earlier for ribonuclease A using urea as the denaturant (*53*). In the presence of 300 mg/mL Ficoll 70, up to 3 M GuHCl does not cause any change in protein secondary structure (Figure S2 of the Supporting Information).

In Figure 1A, we show examples of thermal transitions as a function of Ficoll 70 concentration; in Figure 1B, we plot T_m values (from two-state analysis) as a function of GuHCl concentration and Ficoll 70 level. From the plot, it emerges that cytochrome *c* is stabilized by a few degrees by the presence of Ficoll 70 in a concentration-dependent manner (more Ficoll, higher T_m). Notably, the effect of Ficoll 70 is stronger at higher GuHCl (∼10°) than at lower GuHCl concentrations (2−5°), indicating that when the protein is destabilized, Ficoll 70 can improve cytochrome *c*'s stability. The same thermal midpoints were obtained when using fluorescence (cytochrome *c* has one Trp that is quenched by the heme in the folded, but not in the unfolded, state) as the detection method (not shown).

We also tested the effects of dextran 40 (∼40 kDa) and dextran 70 (∼70 kDa) on cytochrome *c* thermal stability (Figures 1CD). These agents have stabilizing effects on cytochrome *c* thermal stability similar to those of Ficoll 70. Notably, at the lower GuHCl concentrations, the effect of dextran 40 is stronger than that of dextran 70 at the same concentration, implying that the size of the crowding agent matters (smaller is better). Like for Ficoll 70, the effects of dextran 70 and dextran 40 on thermal stability are larger at higher GuHCl concentrations (i.e., when cytochrome *c* is destabilized); this trend is most pronounced for dextran 70 (Figure 1C,D).

The effects on cytochrome *c*'s T_m induced by the presence of macromolecular crowding agents appear primarily due to

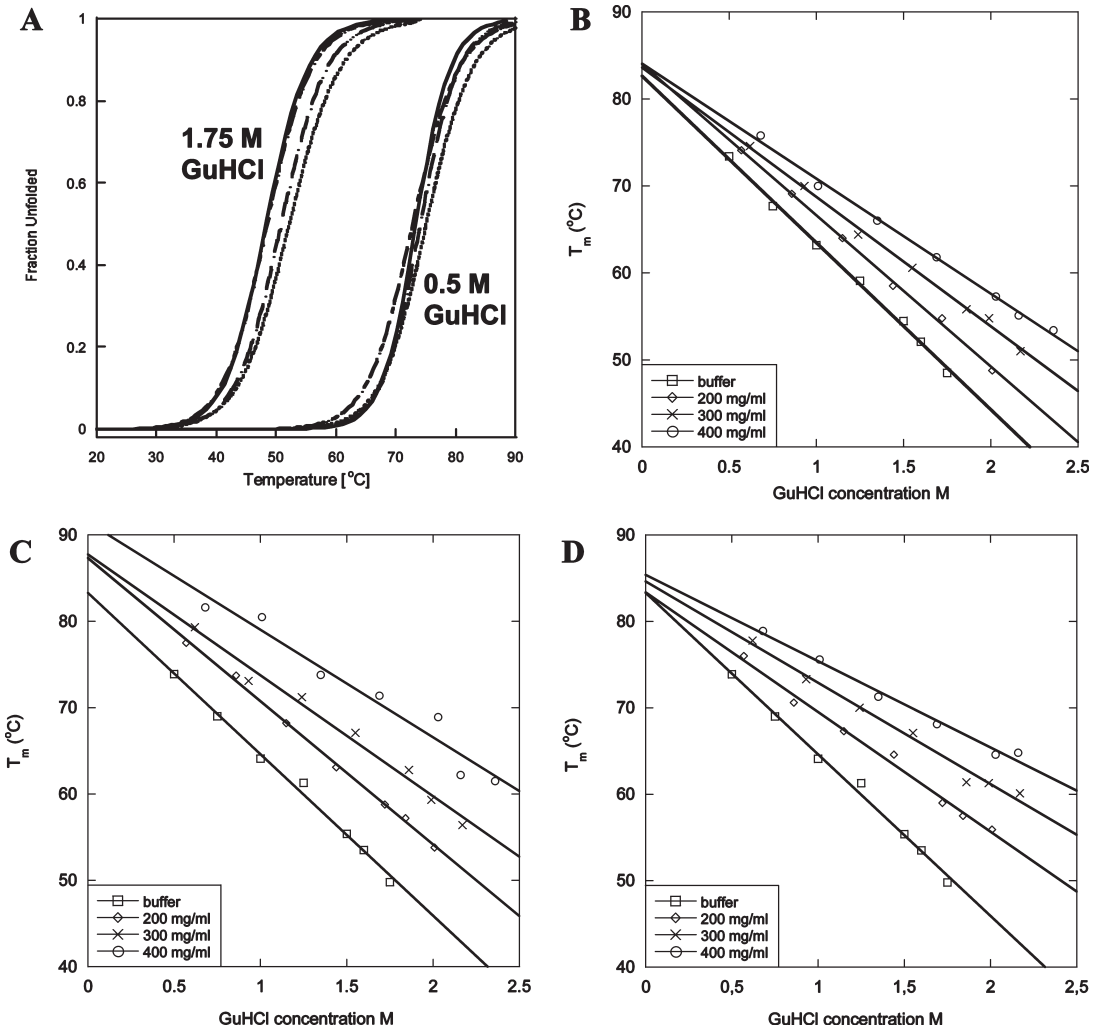

FIGURE 1: Thermal unfolding curves probed by CD at 220 nm as a function of temperature with a scan rate of 1 °C/min. (A) Cytochrome *c* in 0.5 and 1.75 M GuHCl (uncorrected concentration; see Table S1 of the Supporting Information) with 0 (—), 200 (-−-), 300 (·−·), and 400 mg/mL Ficoll 70 (···). (B) T_m values for cytochrome *c* at different corrected GuHCl concentrations with 0, 200, 300, and 400 mg/mL Ficoll 70 (labels for each condition given in each figure). (C) T_m values for cytochrome *c* at different corrected GuHCl concentrations with buffer, 200, 300, and 400 mg/mL dextran 40. (D) T_m values for cytochrome *c* at different corrected GuHCl concentrations with buffer, 200, 300, and 400 mg/mL dextran 70. The values and errors for all T_m values are given in Table S1 of the Supporting Information. Linear fits to the data are only included to "guide the eye".

excluded volume effects (i.e., entropic effects) since the $\Delta H(T_m)$ values at similar GuHCl concentrations are independent (within experimental errors) of crowding agent concentration (Table 1, cf. each horizontal row, which is roughly for the same GuHCl concentration; see Table S2 of the Supporting Information for exact GuHCl values). We note that $\Delta H(T_m)$ should decrease with an increase in GuHCl concentration as the protein is destabilized and $\Delta H(T_m)$ is lowered. This is clearly seen in Table 1 for the buffer column.

Effects of Crowding on Folded- and Unfolded-State Secondary Structures. To test the possible effect of Ficoll 70 and the two dextrans on the folded-state secondary structure content, far-UV CD spectra were recorded as a function of crowding agent additions at 20 °C. For cytochrome *c*, there was no effect of Ficoll 70 or dextran 40 or 70 addition on the protein's secondary structure (i.e., far-UV CD signal) regardless of the presence of low levels of GuHCl (Figure 2A). Moreover, the presence of various crowding agents did not change cytochrome *c*'s Trp fluorescence (Trp environment; data not shown) or visible CD (heme environment; see Figure S2B of the Supporting Information) under any of these GuHCl conditions. This is in contrast to our earlier findings for the larger proteins, apoflavodoxin and VlsE (*20*−*22*). We also analyzed the effect of crowding agents on the thermally unfolded state. For cytochrome *c*, no significant change in unfolded-state secondary structure content (far-UV CD signals collected at 85−90 °C; appropriate baselines subtracted) was found as a function of Ficoll 70 concentration (Figure 2B).

Thermodynamic Analysis of Cytochrome c Behavior in Silico Matches the in Vitro Study. To complement the in vitro data and provide deeper insights into molecular mechanisms, we performed computer simulations on the same protein without and with the inclusion of inert spheres (acting as crowders) of the size of Ficoll 70. As described above, there is no effect of macromolecular crowding on the secondary structure content of the folded and unfolded states of cytochrome *c* in vitro. The same trend is found in silico when analyzing the radius of gyration (R_g) as a function of temperature T (Figure 3A). Crowding has no effect on the sizes of the folded ensemble of cytochrome *c* at low temperatures. There is a 5% reduction in the overall size of the unfolded ensemble at a high temperature in the presence of a high content of Ficoll 70 (ϕ_c = 40%).

In addition, we plotted the folding free energy of cytochrome *c* as a function of the fraction of native contacts (Q) in the presence

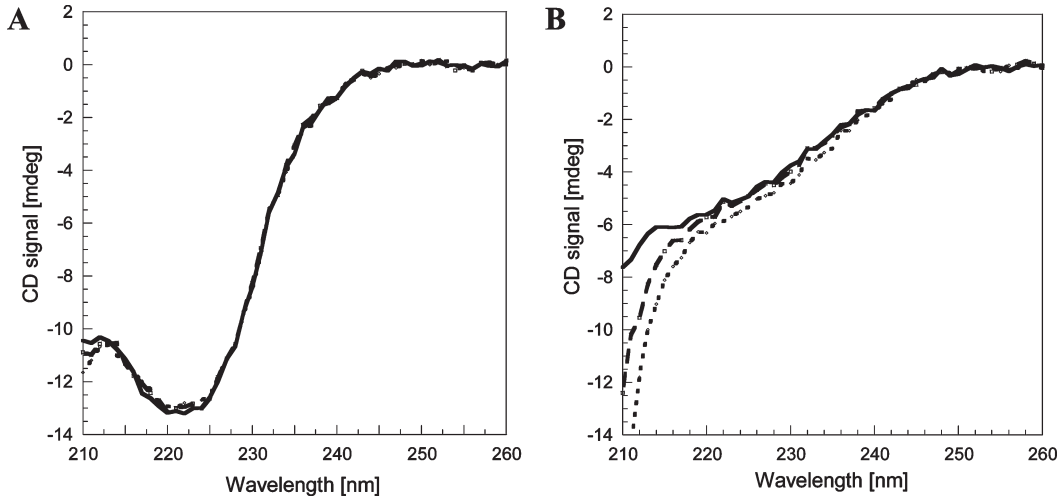

FIGURE 2: Far-UV CD spectra for the folded and unfolded states as a function of added agents at 20 °C. (A) Cytochrome *c* in 0.5 M GuHCl (uncorrected concentration; see Table S1 of the Supporting Information) with 0, 200, 300, and 400 mg/mL Ficoll 70 (all curves overlay). (B) Far-UV CD spectra for unfolded cytochrome *c* with 0 (—), 200 (-−-), and 400 mg/mL Ficoll 70 (···) at 93 °C [0.5 M GuHCl (uncorrected concentration; see Table S1), pH 7].

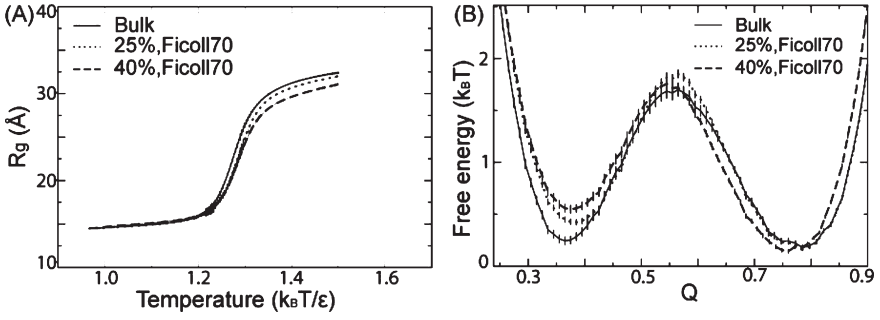

FIGURE 3: (A) Radius of gyration (R_g) vs temperature and (B) free energy landscape of cytochrome *c* as a function of the fraction of native contact formation (Q) at $1.26k_BT/\varepsilon$ in the presence of Ficoll 70 where the volume fraction of crowders, φ_c, equals 0% (bulk), 25%, and 40%. Error bars are indicated in the profiles.

of Ficoll 70 at ϕ_c values of 25 and 40% (Figure 3B). The free energy profiles demonstrate that there is destabilization of the unfolded states in the presence of crowding agents. The change in thermal stability between bulk and φ_c = 40% is small compared to that from our previous study on apoflavoxin (*21*, *33*). The observed small increase in folded-state stability of cytochrome *c* in the presence of Ficoll 70 in silico is in agreement with the in vitro observations of an increased T_m.

In Silico Analysis of the Role of Crowder Size on Cytochrome c. One reason that accounts for a small, or no, effect of crowding on cytochrome *c* may be cytochrome *c* being much smaller than the Ficoll 70 molecules, as suggested by scaled particle theory calculation (*5*). Therefore, we investigated the effects on the thermal stability of cytochrome *c* at a φ_c of 40% using crowders smaller than Ficoll 70 but still spherical [i.e., CR-40, CR-10, and CR-cyt (see Materials and Methods for details)] by computer simulations. Two-dimensional (2D) folding energy landscapes of cytochrome *c* as a function of the radius of gyration (R_g) and the fraction of the native contact formation (Q) at $1.26k_BT/\varepsilon$ are shown in Figure 4 under different crowding conditions [bulk, ϕ_c(Ficoll 70) = 40%, ϕ_c(CR-40) = 40%, ϕ_c(CR-10) = 40%, and ϕ_c(CR-cyt) = 40%]. As the size of a crowder is reduced, cytochrome *c*'s R_g at a low Q (i.e., the unfolded ensemble) decreases drastically, indicating that smaller crowders induced stronger attraction and thereby greater compaction among the unfolded structures.

We also plotted the folding free energy as a function of the fraction of contact formation (Q) (Figure 5). There is a greater destabilization of unfolded states (Q_u = 0.35) as the size of crowder is reduced from Ficoll 70 to CR-10 at a ϕ_c of 40%. Thus, the folded-state stability of cytochrome *c* increases with a decrease in crowder size. Interestingly, with the smallest crowder (CR-cyt), the free energy minimum for the unfolded states increases from a Q_u of 0.35 to a Q_u of 0.4, indicating that the ensemble structures of the unfolded state of cytochrome *c* differ from the other conditions by having more nativelike contacts.

The change in the ensemble structures of unfolded cytochrome *c* at high levels of crowders was further probed by analysis of the differences in the contact formation between a ϕ_c of 40% and a ϕ_c of 0% (bulk) at $1.26k_BT/\varepsilon$. The differences in the probability of native contact formation between a ϕ_c(CR-40) of 40% and bulk, and between a ϕ_c(CR-cyt) of 40% and bulk, in the form of contact maps, are provided in panels A and B of Figure 6, respectively. The top triangle represents hydrogen bond formation and the bottom triangle side chain formation. The region boxed in red, between residue 75 and residue 90, is where the side chain contacts are mostly affected by crowding, particularly by using the smallest crowder, CR-cyt. This region is projected on a crystal structure of cytochrome *c* in red (Figure 6E).

In Silico Analysis of the Role of Crowder Shape on Cytochrome c. At a high level of crowding agents, the geometry of a void formed under crowder density fluctuations plays a key

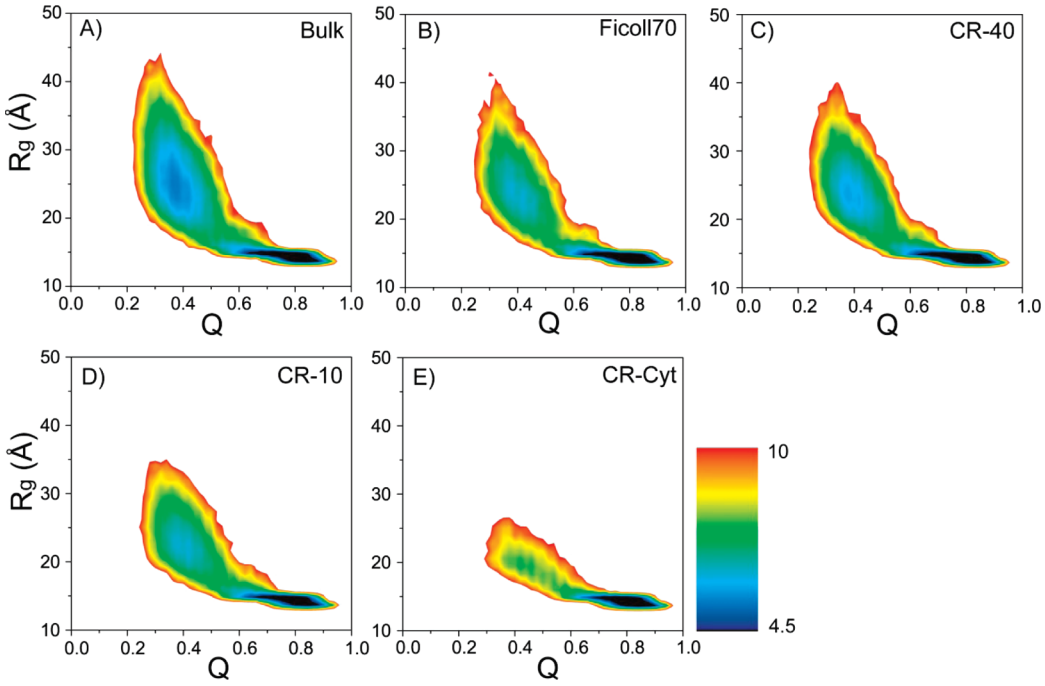

FIGURE 4: 2D folding energy landscape of cytochrome *c* as a function of the radius of gyration (R_g) and the fraction of native contact formation (Q) at $1.26k_BT/\varepsilon$ under the following conditions: (A) $\varphi_c = 0$ (bulk), (B) φ_c(Ficoll 70) = 40%, (C) φ_c(CR-40) = 40%, (D) φ_c(CR-10) = 40%, and (E) φ_c(CR-cyt) = 40%. The free energy is color-scaled by k_BT, and k_B is Boltzmann's constant.

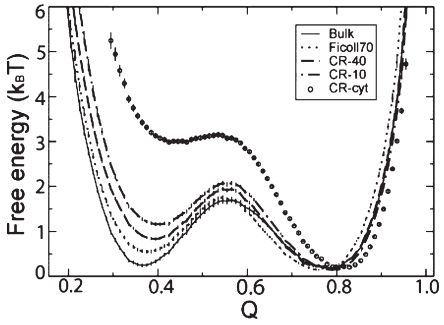

FIGURE 5: Folding energy landscape of cytochrome *c* at $1.26k_BT/\varepsilon$ as a function of the fraction of native contact formation (Q) under the following conditions: bulk (—), φ_c(Ficoll 70) = 40% (···), φ_c(CR-40) = 40% (---), φ_c(CR-10) = 40% (·-·), and φ_c(CR-cyt) = 40% (●).

role in the distribution of ensemble structures of proteins (*33*). Therefore, the shape of the crowding agents may matter with respect to the overall protein biophysical properties. Motivated by the fact that the in vitro thermal stability increases caused by dextran, whose structure at most can be described as anisotropic, are somewhat greater than those caused by Ficoll, we tested two different anisotropic crowders in silico. To address the thermal stability of cytochrome *c* at high levels of anisotropic crowding agents, we adopted two types of dumbbell crowders as simple mimics of dextran: dumbbell70 and SD70 (see Materials and Methods). The latter type of dumbbell, SD70, has a volume equivalent to a single Ficoll 70, whereas the volume of dumbbell70 is double that of one Ficoll 70. Although SD70 is smaller than dumbbell70, all investigations were conducted at the same level of crowding in terms of volume fraction (ϕ_c = 40%).

The radius of gyration (R_g) as a function of temperature is shown in Figure 7A. At high temperatures, greater than the folding temperature (T_f), the R_g of cytochrome *c* in the presence of SD70 is shorter than that in the presence of Ficoll 70. In addition, the R_g of cytochrome *c* in the presence of Ficoll 70 is shorter than that in the presence of dumbbell70. This suggests that the SD70 crowder exerts greater stabilizing effects over Ficoll 70, which is in agreement with experimental findings. Despite the noticeable difference in R_g at high temperatures when using crowders of different shapes, the changes in the free energy as a function of Q (Figure 7B) are less dependent on crowder shape, as demonstrated by the comparison of the SD70 and Ficoll 70 data.

To evaluate the mechanistic interactions between the protein and the crowders of different shapes, we calculated the shape parameters S and Δ (see Materials and Methods for definitions of S and Δ) of cytochrome *c* at a ϕ_c of 40% (Table 2). In the folded state of cytochrome *c*, Δ = 0.06 and S = 0.02, and the two parameters are not changed by different types of crowders. In the unfolded state of cytochrome *c*, the asphericity ranges from 0.45 to 0.49 and the shape parameter ranges from 0.38 to 0.40. Thus, the unfolded protein chains can be considered elongated objects (prolate) in the presence of all different type of crowders analyzed, and the distribution of conformations is not much dependent on crowder shape. Nonetheless, there is a small increase in the level of asymmetry of the unfolded state of cytochrome *c* when going from spherical to dumbbell-shaped crowders at a ϕ_c of 40% (Table 2).

This finding is in sharp contrast to that of the former study on apoflavodoxin (*33*). Among a cluster of unfolded structures of apoflavodoxin that was characterized as spherical, a distinct population of elongated unfolded conformations existed that facilitated off-pathway folding routes. At high levels of crowding, the population of the two major clusters of the unfolded-state conformations could be dramatically altered by using crowders with different geometries. This was demonstrated by changes of up to 20% in S and up to 40% in Δ, values for the ensemble of unfolded apoflavodoxin upon comparison of dumbbell70 and Ficoll 70 data at the ϕ_c = 40% crowding condition.

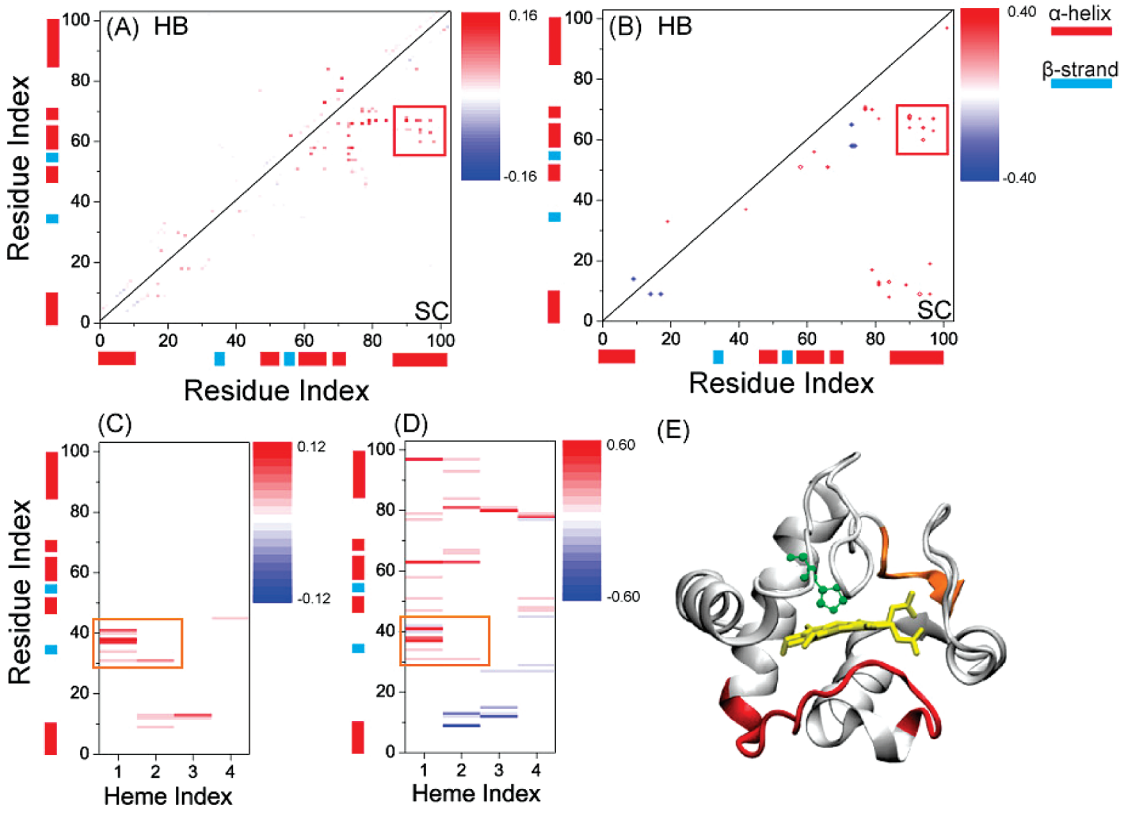

FIGURE 6: Difference in the probability of native contact formation in the unfolded state of cytochrome *c* at $1.26k_BT/\varepsilon$ (A) between a ϕ_c(CR-40) of 40% and bulk and (B) between a ϕ_c(CR-cyt) of 40% and bulk in the form of a contact map. The top triangle represents hydrogen bond formation (HB) and the bottom triangle side chain formation (SC). Contacts defined in a red box are the ones most affected by the high level of crowding. In both contact maps in panels A and B, the secondary structure elements are indicated along with the *x* and *y* axes in which the red segment represents α-helices and the blue ones represents *β*-strands. (C) Differences in the probability of formation of heme−protein contacts between a ϕ_c(CR-40) of 40% and bulk are shown for the unfolded state of cytochrome *c* at $1.26k_BT/\varepsilon$. (D) Same as panel C except it is shown for the simulation between a ϕ_c(CR-cyt) of 40% and bulk. (E) Ribbon illustration of cytochrome *c*. The segment colored red (residues 75−90) is the area for contact formation in the unfolded protein that is most affected by crowding. The segment colored orange (residues 30−40) is the place where contact formation between heme and the unfolded protein is most enhanced by crowding. Heme is colored yellow.

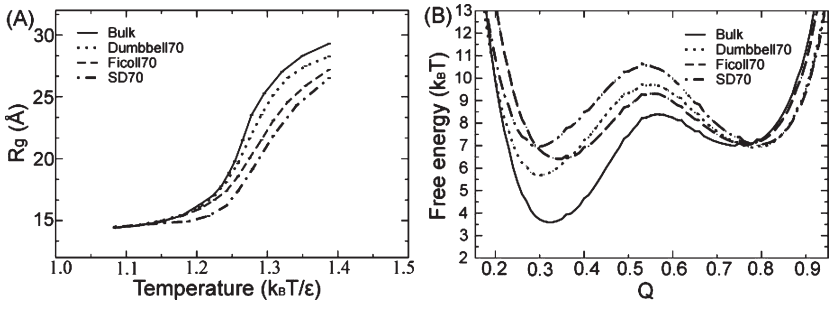

FIGURE 7: In the absence and presence of crowders, (A) the radius of gyration (R_g) vs temperature and (B) the folding energy landscape of cytochrome *c* at $1.28k_BT/\varepsilon$ as a function of the fraction of native contact formation (Q). In both panels: bulk (—), φ_c(dumbbell70) = 40% (···), φ_c(Ficoll 70) = 40% (---), and φ_c(SD70) = 40% (·-·).

Effects of Crowders of Different Shapes on Protein−Heme Interactions. The differences in the probability of the unfolded-state heme−protein contacts between ϕ_c(CR-40) = 40% and bulk (Figure 6C) as well as between ϕ_c(CR-cyt) = 40% and bulk (Figure 6D) are shown as contact maps. In the presence of high levels of crowding, the probability of native contact formation between heme and the protein segment (residues 30−40) clearly increases in the unfolded ensemble of structures (orange segment, Figure 6E). Moreover, the contacts in the orange segment of unfolded cytochrome *c* are more enhanced when a smaller, as compared to larger, spherical crowder was applied.

How the shape of the crowder affects the interactions between the heme and the polypeptide was also investigated (Figure S4 of the Supporting Information). In contrast to the enhanced probability of contacts between the segment of cytochrome *c* (*35*, *40*) and the heme that is proportional to the size of spherical crowders (Figure 6C,D), the same segment (labeled in an orange box in Figure S4), however, was less affected by the dumbbell-shaped crowders. Thus, the geometry of the crowding agents matters for heme−protein contact formation at high levels of crowding. Because folding of cytochrome *c* is believed to start around the heme (*31*), the observed in silico crowding effects on the heme−protein interactions may be important for folding in vivo.

Table 2: Asphericity and Shape Parameters of Cytochrome *c* Ensemble Structures under Bulk Conditions (ϕ_c = 0%) and a ϕ_c = 40% Crowding Condition in the Presence of the Different types of Crowders

	bulk	Ficoll 70	dumbbell70	SD70
		Unfolded		
asphericity (Δ)	0.58 ± 0.00	0.47 ± 0.00	0.49 ± 0.00	0.45 ± 0.00
shape parameter (S)	0.45 ± 0.00	0.39 ± 0.00	0.40 ± 0.00	0.38 ± 0.00
		Folded		
asphericity (Δ)	0.07 ± 0.00	0.06 ± 0.00	0.06 ± 0.00	0.06 ± 0.00
shape parameter (S)	0.03 ± 0.00	0.02 ± 0.00	0.02 ± 0.00	0.02 ± 0.00

DISCUSSION

Here, we report the structural and thermodynamic effects of macromolecular crowding on a helical protein using a combination of in vitro and in silico methods. Whereas we find that folded cytochrome *c* (helical, 104 residues) is not affected structurally (far-UV CD, Trp fluorescence, and heme Soret CD) by crowding, the thermal stability is increased in the presence of crowding agents due to volume exclusion. The in vitro data (structural and thermodynamic) can be reproduced computationally when using a structural based (Go-like) model for cytochrome *c*. We note that a structural (Go-like) potential was successfully applied in studying the folding of cytochrome *c* previously (*31*) .

The results presented here for cytochrome *c* can be compared to those of our previous work, using similar approaches, on the effects of macromolecular crowding on two other apoflavodoxin and VlsE proteins. For apoflavodoxin (α/β structure, 148 residues), we found that macromolecular crowding induces a more ordered, crystal structure-like folded state in solution, along with dramatic increases in thermal stability (*21*). For the *Borrelia* protein VlsE (helical, 328 residues), we found that macromolecular crowding in combination with small perturbations (heat/chemical denaturants) resulted in large structural changes (bending, and more helices, then collapse to a sphere) and a switch in secondary structure content (α to β); this allowed for exposure of a hidden antigen at high crowding levels (*22*). In this work on VlsE (*22*), we adopted a statistical potential that allows attractive non-native interactions in a coarse-grained protein model. For apoflavodoxin (*21*), we used a structure-based (Go-like) model to successfully capture the in vitro data on this protein under crowded conditions and to explain in vitro changes in the folding routes upon mutation (*33*). We note that there are a number of other studies that have also addressed the effects of macromolecular crowding on protein biophysical properties (*10*−*19*).

Role of Protein Size, Shape, and Stability for the Effects of Macromolecular Crowding. Together with our earlier study on the thermal stability of the larger apoflavodoxin, in the presence of the same type of crowder (Ficoll 70), the native-state stability of apoflavodoxin is enhanced ($\Delta\Delta G_{fu}/kT_f = -2.3$; ΔT_f = 19 K from bulk to ϕ_c = 40%) to a greater extent than that of cytochrome *c* ($\Delta\Delta G_{fu}/kT_f = -0.4$; ΔT_f = 4 K from bulk to ϕ_c = 40%) by crowding agents in silico. Experimentally, apoflavodoxin stability was enhanced by up to 20 °C (*21*), whereas cytochrome *c* is stabilized by 5 °C with Ficoll 70 (at 0.5 M GuHCl). Such distinct effects on protein stability with the same crowding content can be explained by a larger destabilization of the unfolded state of apoflavodoxin than that of cytochrome *c* under crowded conditions. In addition, apoflavodoxin's folded-state secondary structure content was modulated by Ficoll 70, which could add to the favorable thermal effect; this was not the case for the folded structure of cytochrome *c* (Figure 2A).

This difference between the two proteins can also be partly explained by scaled particle theory (SPT) (*5*) in which the ratio of the sizes of Ficoll 70 and folded proteins and the ratio of the sizes of Ficoll 70 and unfolded proteins are important factors in determining the extent of macromolecular crowding effects on the protein's stability. As the size of unfolded apoflavodoxin (37.6 Å) is much closer to the size of Ficoll 70 (55 Å) than that of unfolded cytochrome *c* (27.3 Å), it is reasonable that macromolecular crowding has a greater effect on apoflavodoxin's unfolded-state ensemble and thereby on thermal stability.

Cytochrome *c* is spherical as is flavodoxin, whereas VlsE adopts an elongated shape. Taken together with our earlier findings on apoflavodoxin and VlsE, it appears that the more anisotropic a protein is, the stronger the crowding effects [VlsE was found to change shape and collapse into a sphere at high levels of crowding (*22*)]. Moreover, another factor that determines the extent of crowding effects may be protein stability. Cytochrome *c* is more stable than VlsE and apoflavodoxin in vitro, suggesting that the more stable a protein is, the weaker the effects of crowding appear to be (i.e., weakest effects found for the most stable cytochrome *c*). This idea is directly shown here in the fact that the thermal effects on cytochrome *c* of crowding agents increased as a function of increasing GuHCl concentrations that destabilize the protein (Figure 1). We note that another explanation for the trend of an increasing crowding effect at higher GuHCl concentrations may be that the unfolded state of cytochrome *c* becomes more expanded at higher denaturant concentrations (proposed in ref *54*), enhancing the effect of excluded volume.

Role of Crowder Size for the Effects of Macromolecular Crowding on Cytochrome c. The results from our computer simulations of varying spherical crowder sizes were compared with the SPT calculation. We used both Zhou's (*55*) and Minton's SPT models (*5*). For the effective radius of a hard sphere representing the unfolded states of cytochrome *c*, we used 35.2 Å from Minton's formula in ref *5*. This value is the multiplication of $(5/3)^{1/2}$ with the ensemble average (R_g^U) of the unfolded states (i.e., 27.3 Å) measured at a Q_u of 0.3−0.4 at the folding temperature in our computer simulations. For the effective radius of a hard sphere representing the folded states, we used 18.6 Å; this is a multiplication of $(5/3)^{1/2}$ with the ensemble average (R_g^N) of the folded states (i.e., 14 Å) measured at a Q_f of 0.75−0.85 at the folding temperature in our computer simulations. The major difference between the two SPT models is how unfolded states are treated in their calculations of $\Delta\Delta G_{fu}$, the protein stability change due to crowding at a given φ_c (*5*). In Zhou's SPT calculations, unfolded states are soft and modeled as Gaussian chains, whereas in Minton's SPT calculations, unfolded states are modeled as hard cores.

When using Zhou's SPT formula, there is a nonmonotonic trend in which the folding stability of cytochrome *c* first increases inversely with crowder size and then decreases after the crowder size becomes smaller than ~45 Å at a φ_c of 40% (Figure S5A of the Supporting Information). When the crowder size is smaller than 32 Å, $\Delta\Delta G_{fu}$ calculated from Zhou's SPT formula becomes positive. In our coarse-grained molecular simulations using a structural (Go-like) potential, $\Delta\Delta G_{fu}$ is 1 order of magnitude greater than that from Zhou's SPT calculations. In addition, $\Delta\Delta G_{fu}$ from our simulations increases as the crowder size

decreases. The smallest crowder model we used in our study is the size of folded cytochrome *c* (CR-cyt; R_g = 13.1 Å). Meanwhile, $\Delta\Delta G_{fu}$ computed from Minton's SPT formula (Figure S5B of the Supporting Information) is 10 times larger than the values from our computer simulations but follow the same trend as our data. This difference between the two SPT models may arise from the way they model the unfolded states. In Zhou's SPT calculation, the stability of the folded state is unfavorably affected in the presence of crowders by an overestimation of the unfolded-state stability since the unfolded protein chains are allowed to overlap themselves and pass through the space of the crowders. However, in Minton's SPT calculation, the stability of the folded state may be somewhat overestimated since the unfolded-state ensemble is treated as impenetrable hard cores. Our results for crowder size effects on cytochrome *c* stability are in good agreement in a narrow range of crowders whose sizes are larger than the folded protein (data not shown) with another computational study of three different proteins also using Go models (*56*).

Role of Crowder Shape in the Effects on Cytochrome c. In the presence of high levels of macromolecular crowding, the folded-state stability of a protein will depend on many factors, in addition to the excluded volume effects of the crowders. For example, in our prior study on apoflavodoxin, the ensemble structures of folded and unfolded states were modulated by mechanistic interactions between the protein and the crowder molecules (*21*). As a result, the folded state could not be modeled as a hard core. When we subsequently studied the folding routes of apoflavodoxin, the folding mechanism of which involves nonproductive folding pathways due to topological frustrations (*33*), the use of rod-shaped (instead of spherical) crowders was found to alter the distribution of protein conformations in the ensemble such that nonproductive folding route pathways were reduced (*33*).

We here used two different types of rod-shaped (dumbbell) crowders as in silico simple models for dextran 70. Dextran preparations are often polydisperse (*57*, *58*), and their most probable geometry in solution is still under debate (*59*). Nonetheless, dextran is often considered to be rod-shaped (or, an array of smaller rods) in solution (*5*, *60*). Our results for cytochrome *c* using dumbbell crowders were different from our previous results on apoflavodoxin (*33*). In addition, the $\Delta\Delta G_{fu}$ of cytochrome *c* fitted by SPT as a function of the size of spherical crowders qualitatively agrees with the ones calculated from the computer simulations, while SPT is unlikely to explain the behavior of apoflavodoxin. These discrepancies between cytochrome *c* and apoflavodoxin in terms of crowding effects may not be surprising, because cytochrome *c* is smaller than apoflavodoxin and the ensemble structures of folded and unfolded cytochrome *c* are not far from hard-core models.

With the use of the SPT argument, an anisotropic crowder with the same volume as a spherical crowder will exert a greater amount of excluded volume (*61*). Therefore, it explains the observed increases in the folding stability of cytochrome *c* in the presence of dextran 70 over Ficoll 70. In contrast, dumbbell70, having a larger volume per crowder than either Ficoll 70 or SD70, produces the greateast probable void size among the three crowder models in our simulations. This leads to the least impact on the folding stability of cytochrome *c*.

There is another reason that SPT fits the behavior of cytochrome *c*, but not that of apoflavodoxin: the fact that the folding mechanism of cytochrome *c* does not involve topological frustration. In the case of apoflavodoxin, competing folding routes led to off-pathway folding intermediates that competed with productive folding. This behavior is not found in the folding landscape of cytochrome *c* (data not shown; see also ref *31*). Instead, the folding behavior of cytochrome *c* in silico is similar to that of protein systems used in other studies that fit with various SPT models (*5*, *56*).

CONCLUSIONS

Proteins fold in a cell's environment that is crowded with macromolecules. It is therefore important to understand, on a molecular level, how this exclusion of volume affects protein biophysical properties in comparison to their behaviors in conventional experiments performed in dilute buffers in vitro. We here tested the effect of macromolecular crowding agents (mimicking the crowdedness of the cell) on a small model protein, cytochrome *c*, using in vitro and in silico methods. We found, in contrast to earlier studies on two other model systems (the larger proteins apoflavodoxin and VlsE), that the folded-state structure of cytochrome *c* is not perturbed under crowded conditions. However, in accord with findings on other proteins and excluded volume theory, cytochrome *c* is thermally stabilized under crowded conditions. Analysis of our data reveals that this is an entropic effect due to compaction of the unfolded state. When cytochrome *c* is destabilized (by inclusion of low levels of chemical denaturant), the stabilizing effect of crowding increases, implying that the less stable a protein is, the larger the possible effect of crowding. This also agrees with earlier work on apoflavodoxin and VlsE; both proteins are less stable in vitro than cytochrome *c*, and in both cases, we observed folded-state secondary structure changes under crowded conditions. Another factor that appears to dictate the magnitude of the effect of crowding is the relative size of the protein and crowder. When these two sizes come closer to each other, the effect of crowding on cytochrome *c*'s thermal stability increases. A third factor that can influence the effects of macromolecular crowding is crowder geometry. Given the same high volume fraction φ_c and number density ρ_c, we find that an anisotropic crowder will enhance protein stability more than a spherical crowder.

In summary, we have identified the protein stability, crowder-to-protein size ratio, geometry of crowders, and topological frustration during protein folding as key factors defining the net effect of excluded volume on protein biophysics. Further studies on other protein systems with varying size, structure, and stability are needed to confirm these conclusions. In addition, it will be important to test the effect of heterogeneous mixtures of crowders to better mimic the in vivo condition.

ACKNOWLEDGMENT

We thank Dr. D. Homouz for helpful suggestions on the manuscript and the Texas Advanced Computing Center as well as the Texas Learning and Computation Center at the University of Houston for computational resources.

SUPPORTING INFORMATION AVAILABLE

Figures S1−S5 and Tables S1−S3. This material is available free of charge via the Internet at http://pubs.acs.org.

REFERENCES

1. Rivas, G., Ferrone, F., and Herzfeld, J. (2004) Life in a crowded world. *EMBO Rep. 5*, 23–27.
2. Ellis, R. J., and Minton, A. P. (2003) Cell biology: Join the crowd. *Nature 425*, 27–28.

3. Minton, A. P., and Wilf, J. (1981) Effect of macromolecular crowding upon the structure and function of an enzyme: Glyceraldehyde-3-phosphate dehydrogenase. *Biochemistry 20*, 4821–4826.
4. Laurent, T. C., and Ogston, A. G. (1963) The Interaction between Polysaccharides and Other Macromolecules. 4. The Osmotic Pressure of Mixtures of Serum Albumin and Hyaluronic Acid. *Biochem. J. 89*, 249–253.
5. Minton, A. P. (2005) Models for excluded volume interaction between an unfolded protein and rigid macromolecular cosolutes: Macromolecular crowding and protein stability revisited. *Biophys. J. 88*, 971–985.
6. Zhou, H. X. (2004) Loops, linkages, rings, catenanes, cages, and crowders: Entropy based strategies for stabilizing proteins. *Acc. Chem. Res. 37*, 123–130.
7. Cheung, M. S., Klimov, D., and Thirumalai, D. (2005) Molecular crowding enhances native state stability and refolding rates of globular proteins. *Proc. Natl. Acad. Sci. U.S.A. 102*, 4753–4758.
8. Harve, K. S., Lareu, R., Rajagopalan, R., and Raghunath, M. (2010) Understanding how the crowded interior of cells stabilizes DNA/DNA and DNA/RNA hybrids: In silico predictions and in vitro evidence. *Nucleic Acids Res. 38*, 172–181.
9. Eggers, D. K., and Valentine, J. S. (2001) Crowding and hydration effects on protein conformation: A study with sol-gel encapsulated proteins. *J. Mol. Biol. 314*, 911–922.
10. Cheung, M. S., and Thirumalai, D. (2007) Effects of crowding and confinement on the structures of the transition state ensemble in proteins. *J. Phys. Chem. B 111*, 8250–8257.
11. Homouz, D., Sanabria, H., Waxham, M. N., and Cheung, M. S. (2009) Modulation of calmodulin plasticity by the effect of macromolecular crowding. *J. Mol. Biol. 391*, 933–943.
12. Zhang, S. Q., and Cheung, M. S. (2007) Manipulating biopolymer dynamics by anisotropic nanoconfinement. *Nano Lett. 7*, 3438–3442.
13. Qin, S., and Zhou, H. X. (2009) Atomistic modeling of macromolecular crowding predicts modest increases in protein folding and binding stability. *Biophys. J. 97*, 12–19.
14. Mittal, J., and Best, R. B. (2008) Thermodynamics and kinetics of protein folding under confinement. *Proc. Natl. Acad. Sci. U.S.A. 105*, 20233–20238.
15. Wang, W., Xu, W. X., Levy, Y., Trizac, E., and Wolynes, P. G. (2009) Confinement effects on the kinetics and thermodynamics of protein dimerization. *Proc. Natl. Acad. Sci. U.S.A. 106*, 5517–5522.
16. Griffin, M. A., Friedel, M., and Shea, J. E. (2005) Effects of frustration, confinement, and surface interactions on the dimerization of an off-lattice β-barrel protein. *J. Chem. Phys. 123*, 174707.
17. McGuffee, S. R., and Elcock, A. H. (2006) Atomically detailed simulations of concentrated protein solutions: The effects of salt, pH, point mutations, and protein concentration in simulations of 1000-molecule systems. *J. Am. Chem. Soc. 128*, 12098–12110.
18. Dedmon, M. M., Patel, C. N., Young, G. B., and Pielak, G. J. (2002) FlgM gains structure in living cells. *Proc. Natl. Acad. Sci. U.S.A. 99*, 12681–12684.
19. Sasahara, K., McPhie, P., and Minton, A. P. (2003) Effect of dextran on protein stability and conformation attributed to macromolecular crowding. *J. Mol. Biol. 326*, 1227–1237.
20. Perham, M., Stagg, L., and Wittung-Stafshede, P. (2007) Macromolecular crowding increases structural content of folded proteins. *FEBS Lett. 581*, 5065–5069.
21. Stagg, L., Zhang, S. Q., Cheung, M. S., and Wittung-Stafshede, P. (2007) Molecular crowding enhances native structure and stability of α/β protein flavodoxin. *Proc. Natl. Acad. Sci. U.S.A. 104*, 18976–18981.
22. Homouz, D., Perham, M., Samiotakis, A., Cheung, M. S., and Wittung-Stafshede, P. (2008) Crowded, cell-like environment induces shape changes in aspherical protein. *Proc. Natl. Acad. Sci. U.S.A. 105*, 11754–11759.
23. Miller, G. L. (1959) Use of dinitrosalicylic acid reagent for determination of reducing sugar. *Anal. Chem. 31*, 426–428.
24. Ramsay, G., and Eftink, M. (1994) Analysis of multidimensional spectroscopic data to monitor unfolding of proteins. *Methods Enzymol. 240*, 615–645.
25. Greenfield, N. (2006) Using circular dichroism collected as a function of temperature to determine the thermodynamics of protein unfolding and binding interactions. *Nat. Protoc. 1*, 2527–2535.
26. Pace, C. N., and Shaw, K. L. (2000) Linear extrapolation method of analyzing solvent denaturation curves. *Proteins* No. Suppl. 4, 1–7.
27. Hall, D., and Minton, A. P. (2003) Macromolecular crowding: Qualitative and semiquantitative successes, quantitative challenges. *Biochim. Biophys. Acta 1649*, 127–139.
28. Record, M. T., Jr., Courtenay, E. S., Cayley, S., and Guttman, H. J. (1998) Biophysical compensation mechanisms buffering *E. coli* protein-nucleic acid interactions against changing environments. *Trends Biochem. Sci. 23*, 190–194.
29. Cayley, S., Lewis, B. A., Guttman, H. J., and Record, M. T. (1991) Characterization of the cytoplasm of *Escherichia coli* K-12 as a function of external osmolarity: Implications for protein-DNA interactions in vivo. *J. Mol. Biol. 222*, 281–300.
30. Cheung, M. S., Finke, J. M., Callahan, B., and Onuchic, J. N. (2003) Exploring the interplay of topology and secondary structural formation in the protein folding problem. *J. Phys. Chem. B 107*, 11193–11200.
31. Weinkam, P., Zong, C., and Wolynes, P. G. (2005) A funneled energy landscape for cytochrome c directly predicts the sequential folding route inferred from hydrogen exchange experiments. *Proc. Natl. Acad. Sci. U.S.A. 102*, 12401–12406.
32. Sobolev, V., Sorokine, A., Prilusky, J., Abola, E. E., and Edelman, M. (1999) Automated analysis of interatomic contacts in proteins. *Bioinformatics 15*, 327–332.
33. Homouz, D., Stagg, L., Wittung-Stafshede, P., and Cheung, M. S. (2009) Macromolecular crowding modulates folding mechanism of α/β protein apoflavodoxin. *Biophys. J. 96*, 671–680.
34. Case, D. A., Pearlman, D. A., Caldwell, J. W., Cheatham, T. E., Ross, W. S., Simmerling, C. L., Darden, T. A., Merz, K. M., Jr., Stanton, R. V., Cheung, A. L., et al. (1999) AMBER6, University of California, San Francisco.
35. Veitshans, T., Klimov, D., and Thirumalai, D. (1997) Protein folding kinetics: Timescales, pathways and energy landscapes in terms of sequence-dependent properties. *Folding Des. 2*, 1–22.
36. Sugita, Y., and Okamoto, Y. (1999) Replica: Exchange molecular dynamics methods for protein folding. *Chem. Phys. Lett. 314*, 141–151.
37. Frenkel, D., and Smit, B. (2001) Understanding Molecular Simulation: From Algorithms to Applications, Academic Press, New York.
38. Chodera, J. D., Swope, W. C., Pitera, J. W., Seok, C., and Dill, K. A. (2007) Use of the weighted histogram analysis method for the analysis of simulated and parallel tempering simulations. *J. Chem. Theory Comput. 3*, 26–41.
39. Dima, R. I., and Thirumalai, D. (2004) Assymetry in the shapes of folded and denatured states of proteins. *J. Phys. Chem. B 108*, 6564–6570.
40. Pozdnyakova, I., and Wittung-Stafshede, P. (2001) Copper binding before polypeptide folding speeds up formation of active (holo) *Pseudomonas aeruginosa* azurin. *Biochemistry 40*, 13728–13733.
41. Wittung-Stafshede, P. (2004) Role of cofactors in folding of the blue-copper protein azurin. *Inorg. Chem. 43*, 7926–7933.
42. Chen, E., Goldbeck, R. A., and Kliger, D. S. (2004) The earliest events in protein folding: A structural requirement for ultrafast folding in cytochrome c. *J. Am. Chem. Soc. 126*, 11175–11181.
43. Winkler, J. R., Wittung-Stafshede, P., Leckner, J., Malmstrom, B. G., and Gray, H. B. (1997) Effects of folding on metalloprotein active sites. *Proc. Natl. Acad. Sci. U.S.A. 94*, 4246–4249.
44. Wilson, C. J., and Wittung-Stafshede, P. (2005) Role of structural determinants in folding of the sandwich-like protein *Pseudomonas aeruginosa* azurin. *Proc. Natl. Acad. Sci. U.S.A. 102*, 3984–3987.
45. Wilson, C. J., and Wittung-Stafshede, P. (2005) Snapshots of a Dynamic Folding Nucleus in Zinc-Substituted *Pseudomonas aeruginosa* Azurin. *Biochemistry 44*, 10054–10062.
46. Bohrer, M. P., Patterson, G. D., and Carroll, P. J. (1984) Hindered diffusion of dextran and Ficoll in microporous membranes. *Macromolecules 17*, 1170–1173.
47. Davidson, M. D., and Deen, W. M. (1988) Hindered diffusion of water-soluble macromolecules in membranes. *Macromolecules 21*, 3474–3481.
48. Ohlson, M., Sorensson, J., Lindstrom, K., Blom, A. M., Fries, E., and Haraldsson, B. (2001) Effects of filtration rate on the glomerular barrier and clearance of four differently shaped molecules. *Am. J. Physiol. 281*, F103–F113.
49. Oliver, J. D., III, Anderson, S., Troy, J. L., Brenner, B. M., and Deen, W. H. (1992) Determination of glomerular size-selectivity in the normal rat with Ficoll. *J. Am. Soc. Nephrol. 3*, 214–228.
50. Laurent, T. C., and Killander, J. (1964) Theory of gel filtration and its experimental verification. *J. Chromatogr. 14*, 317–330.
51. Xu, Q., and Keiderling, T. A. (2004) Optical spectroscopic differentiation of various equilibrium denatured states of horse cytochrome c. *Biopolymers 73*, 716–726.
52. Valusova, E., Svec, P., and Antalik, M. (2009) Structural and thermodynamic behavior of cytochrome c assembled with glutathione-covered gold nanoparticles. *J. Biol. Inorg. Chem. 14*, 621–630.

53. Tokuriki, N., Kinjo, M., Negi, S., Hoshino, M., Goto, Y., Urabe, I., and Yomo, T. (2004) Protein folding by the effects of macromolecular crowding. *Protein Sci. 13*, 125–133.
54. Tsong, T. Y. (1974) The Trp-59 fluorescence of ferricytochrome c as a sensitive measure of the over-all protein conformation. *J. Biol. Chem. 249*, 1988–1990.
55. Zhou, H. X. (2008) Effect of mixed macromolecular crowding agents on protein folding. *Proteins 72*, 1109–1113.
56. Mittal, J., and Best, R. B. (2010) Dependence of Protein Folding Stability and Dynamics on the Density and Composition of Macromolecular Crowders. *Biophys. J. 98*, 315–320.
57. Granath, K. A. (1958) Solution properties of branched dextrans. *J. Colloid Sci. 13*, 308–328.
58. Ogston, A. G., and Preston, B. N. (1979) The molecular compression of dextran. *Biochem. J. 183*, 1–9.
59. Goins, A. B., Sanabria, H., and Waxham, M. N. (2008) Macromolecular crowding and size effects on probe microviscosity. *Biophys. J. 95*, 5362–5373.
60. Edmond, E., and Ogston, A. G. (1968) An approach to the study of phase separation in ternary aqueous systems. *Biochem. J. 109*, 569–576.
61. Minton, A. P. (1981) Excluded volume as a determinant of macromolecular structure and reactivity. *Biopolymers 20*, 2093–2120.